Multielectron geometric phase in intensity interferometry

Disha Wadhawan,[1,*] Krishanu Roychowdhury,[2,3,†] Poonam Mehta,[4,‡] and Sourin Das[1,5,§]
[1]*Department of Physics and Astrophysics, University of Delhi, Delhi 110007, India*
[2]*LASSP, Department of Physics, Cornell University, Ithaca, New York 14853, USA*
[3]*Kavli Institute for Theoretical Physics, University of California, Santa Barbara, California 93106-4030, USA*
[4]*School of Physical Sciences, Jawaharlal Nehru University, New Delhi 110067, India*
[5]*Department of Physical Sciences, IISER Kolkata, Mohanpur, West Bengal 741246, India*

(Received 3 January 2018; revised manuscript received 4 July 2018; published 5 October 2018)

Pancharatnam's experimental findings on amplitude interferometry of polarized light during 1950's was an early example of the Berry phase. But a similar experimental realization of the geometric phase in the context of solid-state electronic systems where the polarization state of the photon is replaced by spin-polarized states of the electron remains unexplored. This is primarily due to the fact that the generation of Pancharatnam's geometric phase involves a discrete number of cyclic projective measurements on the polarized states of light, and an equivalent cyclic operation on electron spin is much harder to implement in a solid-state setting. In the present paper, we show that the edge states of the quantum spin Hall effect in conjunction with tunnel coupled spin-polarized electrodes (SPEs) provide us with a unique opportunity to generate Pancharatnam's type of geometric phase locally in space, which can be detected via electronic current measurements. We show that the controlled manipulation of the polarization directions of the SPEs results in coherent oscillations in the cross-correlated current noise, which can be attributed to a multiparticle version of Pancharatnam's geometric phase, and is directly related to the phenomenon of intensity interferometry. We demonstrate that the interference patterns produced due to the manipulation of the geometric phase in our proposed setup show a remarkable immunity to orbital dephasing owing to their spatially local origin.

DOI: 10.1103/PhysRevB.98.155113

I. INTRODUCTION

Soon after Berry's seminal work [1] which generated tremendous excitement, it was pointed out by Ramaseshan and Nityananda [2] that the phase factor arising in cyclic changes of the polarization states in Pancharatnam's work [3] on amplitude interferometry was in fact an early example of the Berry phase. Berry translated Pancharatnam's findings in a quantum mechanical language and introduced the Aharonov-Bohm (AB) effect [4] on the Poincaré sphere by exploiting the fact that the polarization of light is isomorphic to a two-level quantum system [5] (see also Ref. [6]). This led to a wide appreciation of Pancharatnam's work in the context of geometric phases in quantum physics.

Concurrent to this, another exciting development occurred due to Hanbury Brown and Twiss (HBT), who replaced Michelson interferometry by intensity interferometry while measuring the diameter of stars [7]. Intensity interferometry essentially refers to processes in which a pair of particles interferes with itself. In the context of optics, a generalization of the HBT experiment was recently proposed [8] (a simpler setup has been proposed recently in Ref. [9]) which was carried out in Refs. [10,11]. It was shown that the vector nature of light introduces a nonlocal and multiparticle geometric component in addition to the usual dynamical component in the HBT correlation.

In the context of electronic charge transport, a nonlocal and multiparticle AB effect has been observed in experiments involving edge currents in quantum Hall systems [12] (see Ref. [13] for pertinent theoretical developments). However, it should be noted that only the coupling to the orbital degrees of freedom of electrons was exploited in Ref. [12] and the spin remained frozen.

In the present proposal, we demonstrate a way to exploit the spin degrees of freedom of the electrons in order to generate the AB effect in spin space. To illustrate the idea of the AB effect in spin space, let us consider a standard two-path interferometer [14] as a prototype. Let us further assume that the interferometer arms are endowed with the possibility of rotating the electron spin [15] as it traverses through the respective arms [see Fig. 1(a)] of the interferometer. Hence, when an electron with its spin polarized along a given z axis (call it $|\uparrow\rangle$) is incident on the interferometer, its amplitude of propagation will split into two parts, with each part traversing coherently along the respective arm. Finally, these two amplitudes are made to interfere, producing a resulting intensity at the other end of the interferometer. Now, if we assume that the arms of the interferometer are of identical lengths with no net magnetic flux being enclosed, one would expect a perfect constructive interference.

However, the situation changes if we allow for a rotation of the electron spin along each arm. It turns out that the

*dwadhawan@physics.du.ac.in
†kr366@cornell.edu
‡pm@jnu.ac.in
§sourin@iiserkol.ac.in

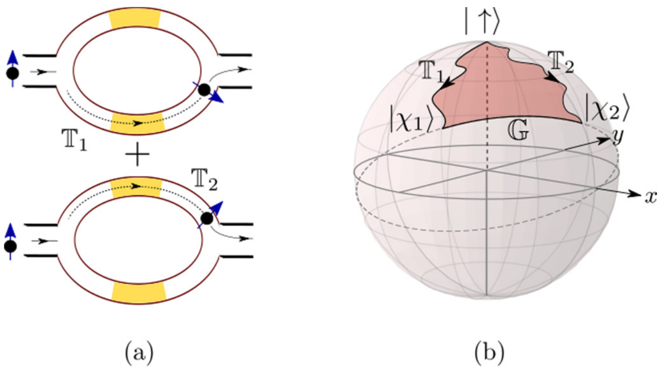

FIG. 1. (a) Schematic of the setup to realize the one-particle spin AB effect. The two interfering paths are depicted as $\mathbb{T}_1$ and $\mathbb{T}_2$ and the yellow shades represent the region of rotation of spin. (b) The trajectories $\mathbb{T}_1$ and $\mathbb{T}_2$ represent the evolution of spin on the Bloch sphere. The geodesic $\mathbb{G}$ connects the end points, forming a closed AB loop surrounding the red shaded region.

spin dynamics alone can generate a nontrivial interference pattern which can be visualized as an AB effect on the Bloch sphere [16]. Due to the spin-active interferometer arms, the incident electron with spin $|\uparrow\rangle$ evolves into $|\chi_1\rangle$ (lower arm) or $|\chi_2\rangle$ (upper arm) as it traverses the respective arm. Hence, traversing through the lower or the upper arm actually traces out two independent trajectories [labeled $\mathbb{T}_1$ and $\mathbb{T}_2$ in Fig. 1(a)] starting from the same point corresponding to the incident state $|\uparrow\rangle$ on the Bloch sphere. Following Ref. [5], the resulting interference pattern will depend on an extra phase factor which is given by half the solid angle subtended at the center by the closed area surrounded by $\mathbb{T}_1$, $\mathbb{T}_2$ and the geodesic [17] $\mathbb{G}$ connecting $|\chi_1\rangle$ and $|\chi_2\rangle$ on this Bloch sphere. This phase is the same as the AB phase accumulated by an electron while traversing once around the periphery of the above-defined area ($\mathcal{A}\{\mathbb{T}_1,\mathbb{T}_2,\mathbb{G}\}$) on the surface of a unit sphere [see Fig. 1(b)]. This can be interpreted as if a (hypothetical) monopole of half strength is sitting at the center of this sphere [1]. Hence this is referred to as an AB effect on the Bloch sphere and the tunability of spin results in a modulation of the phase which can be observed as oscillations when we change $\mathbb{T}_1$ or $\mathbb{T}_2$ or both in a controlled manner.

A setup involving the two-path interferometer-type geometry which could produce such a type of geometric phase from electronic spin dynamics has been explored extensively in the past by Loss *et al.* [18] and Stern [19]. In their work, the geometric phase was induced by an arbitrary smooth closed loop evolution of the spin on the Bloch sphere. To this end, a question that naturally arises in the first place is if one could produce as well this type of geometric phase in a controlled fashion resulting purely from the evolution of the electron spin only along geodesic paths on the Bloch sphere, which will be a step beyond Refs. [18,19]. This will be a proper analog of Pancharatnam's geometric phase [17], which can be visualized by considering a closed loop evolution of spins on the Bloch sphere discretized in a set of n ($n > 2$) number of points on the Bloch sphere connected via geodesics, hence forming a spherical polygon.

In view of the above discussion, the questions that we address in this paper are as follows: (a) Can we produce such a geometric phase locally in space and control it in a desired fashion without introducing an interferometer type setup, (b) if (a) is a success, will there be any observable consequences, and finally, (c) can we produce a multielectron (in our case a two-electron HBT-type [7]) analog (where the loop on the Bloch sphere is closed by spin evolution of not one but two electrons simultaneously) of a Pancharatnam-type geometric phase which is generated locally in space and measurable via standard protocols that are routinely used in electrical transport experiments in mesoscopic systems.

The organization of the paper is as follows. In Sec. II, we introduce the model for amplitude interferometry and answer questions (a) and (b) raised above. Here, we illustrate how the Pancharatnam phase manifests as oscillations in measurable physical quantities. In Sec. III, we discuss its multielectron realization in the context of intensity interferometry as framed in question (c) above. We also remark on the robust nature of the oscillations and their immunity against orbital dephasing by including an extended tunnel junction in the intensity interferometer where phase averaging is introduced to mimic orbital dephasing. We finally conclude in Sec. IV, summarizing all the results.

II. PANCHARATNAM PHASE IN AMPLITUDE INTERFEROMETRY

First, in order to address questions (a) and (b), we study a setup comprising helical edge states (HESs) of a quantum spin Hall state (QSHS) [20–23] locally tunnel coupled to a single spin-polarized electrode (SPE) which facilitates spin injection on the edges as well as supports their reflection back [see Fig. 2(a)]. Here, the QSHS is hosted on the x-y plane, and the spins of the helical edge states are assumed to be polarized along the z axis with S_z being conserved [24]. In order to realize the Pancharatnam phase in this setup, the time-reversal symmetry must be broken on the edges. We will illustrate this point further when we calculate measurable quantities such as current and noise in the setup.

In the presence of an in-plane magnetic field, the HES spectrum gets gapped. We sustain electronic transport in the system when we place the chemical potential (μ) in the conduction band [25] (see Fig. 2). The dynamics of the new edge states is then effectively described by the Hamiltonian (assuming an intrinsic coordinate x along the edge), which is valid within a linearization bandwidth about μ, given by

$$\mathcal{H}_0 = -\imath\hbar v_F \int_{-\infty}^{\infty} dx(\psi_R^\dagger\partial_x\psi_R - \psi_L^\dagger\partial_x\psi_L), \tag{1}$$

where v_F is the renormalized Fermi velocity decided by μ and the magnetic field, and the operators $\psi_R^\dagger$ and $\psi_L^\dagger$ create electrons, respectively, for the right (R) and the left (L) propagating electron states with the spinor part of the normalized wave function given by $|n_R\rangle$ and $|n_L\rangle$. Note that $\langle n_L|n_R\rangle \neq 0$ (see Fig. 2) as time-reversal symmetry is broken.

For simplicity, we model the SPE as a one-dimensional system on a half line (extended from $-\infty$ to 0) whose spectrum is linearized about its Fermi energy, and an unfolding trick [26] is used to describe it as a right moving chiral mode (R') extended from ($-\infty$ to ∞) with a specific spin polarization given by the spinor $|n_{R'}\rangle$. The corresponding

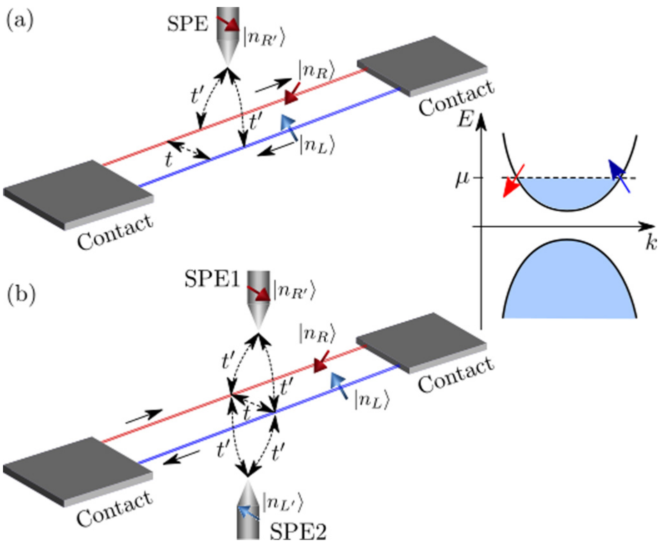

FIG. 2. The cartoon picture of the energy spectrum for the helical edge state, when exposed to an external magnetic field, is presented on the right-hand side of the figure. Here, the red and blue arrows represent the spin polarization directions of left and right movers. (a) A cartoon picture of the setup for amplitude interferometry in which the HES (which has a dispersion as shown on the right-hand side of the figure) is tunnel coupled to a SPE that facilitates injection of a fully polarized electron onto the helical edges. Here, t is the intraedge scattering amplitude while t' is the tunneling amplitude between the SPE and the helical edge states. (b) The cartoon picture of the setup for intensity interferometry where tunneling of electrons happens simultaneously between the helical edge state and the two SPEs. The (single-headed) black arrows on the edges represent the direction of motion of the electrons with a given spin.

Hamiltonian is then given by

$$\mathcal{H}_{\rm SPE} = -\imath\hbar v_F \int_{-\infty}^{\infty} dx \psi_{R'}^{\dagger}\partial_x\psi_{R'}. \tag{2}$$

We further allow for weak tunneling of electrons between the SPE and the edges.

A finite but small backscattering within the edges is assumed to exist essentially because of the possible presence of a fringing field due to the proximity of the ferromagnetic lead. We consider a situation where the tunneling between the SPE and the edges is local in space and it is taking place at $x = 0$ [Fig. 2(a)]. Hence, the tunneling Hamiltonian is given by

$$\mathcal{H}_T = \int_{-\infty}^{\infty} dx\, \delta(x)\left\{\sum_{\eta,\eta',\eta\neq\eta'} t_{\eta\eta'}\psi_\eta^{\dagger}\psi_{\eta'} + \text{H.c.}\right\}, \tag{3}$$

where $\eta, \eta' \in \{R, L, R'\}$ and $t_{\eta\eta'}$ is the tunneling strength between η and η', further expressed as $t_{\eta\eta'} = \tilde{t}\gamma_{\eta\eta'}$ with $\gamma_{\eta\eta'} \equiv \langle n_\eta|n_{\eta'}\rangle$. We take the choice $\tilde{t} = t$ for $\eta, \eta' \in \{R, L\}$ (i.e., the backscattering) and $\tilde{t} = t'$ otherwise (i.e., tunneling between the SPE and the edges). Later, we will consider the case of an extended tunnel junction in the presence of dephasing and show that our results are robust to such a consideration.

We now introduce the scattering matrix (or S matrix) that describes the junction between the HES and the SPE with the total Hamiltonian

$$\mathcal{H} = \mathcal{H}_0 + \mathcal{H}_{\rm SPE} + \mathcal{H}_T. \tag{4}$$

The incident wave function from either the left contact or right contact or the SPE on the tunnel junction at $x = 0$ is transmitted and reflected as an outgoing wave function. If the wave functions associated with the incoming and the outgoing channels are given by $\psi_\eta^{\rm in}$ and $\psi_\eta^{\rm out}$, respectively, then the corresponding S-matrix elements are defined through

$$\psi_\eta^{\rm out} = \sum_{\eta'} s_{\eta\eta'}\, \psi_{\eta'}^{\rm in}. \tag{5}$$

We shall show below that in the presence of finite backscattering ($t \neq 0$), both the current and the cross-correlated noise would feature oscillations arising purely from tuning the geometric phase associated with the area of the Pancharatnam loops on the Bloch sphere, which were absent for $t = 0$. For an explicit calculation of the S-matrix elements, refer to the Appendices A and B and Ref. [27].

We consider a situation where the HES of QSHS is connected to left and right contacts which are grounded, i.e., $V_R = V_L = 0$ ($V_{L/R}$ are the voltages applied on the left and right contacts) while the SPE is maintained at a bias voltage $V_{R'} = V$. In this situation the part of the total injected current into HES moving towards the left or right becomes $\langle I_\eta^{\rm out}\rangle = \frac{e^2V}{h}|s_{\eta R'}|^2$, where $\eta = L/R$. In the weak tunneling limit between the SPE and the edge states ($t' \ll \hbar v_F$) we expand the current $\langle I_\eta^{\rm out}\rangle$ perturbatively up to leading order in t' to obtain

$$\begin{aligned}\left\langle I_{(R/L)}^{\rm out}\right\rangle = \frac{e^2V}{h}t'^2 A\big\{&t^2|\gamma_{RL}|^2|\gamma_{(L/R)R'}|^2 + 4\hbar^2 v_F^2|\gamma_{(R/L)R'}|^2\\ &+ 4\zeta_{(R,L)}tz\hbar v_F\sin(\Omega/2)\big\},\end{aligned} \tag{6}$$

in the zero-temperature limit, where $A = 4/(4\hbar^2v_F^2 + t^2|\gamma_{LR}|^2)^2$, $\gamma_{RL} = \langle n_R|n_L\rangle$, $\gamma_{RR'} = \langle n_R|n_{R'}\rangle$, $\gamma_{R'L} = \langle n_{R'}|n_L\rangle$, $\zeta_R = 1$, $\zeta_L = -1$, and $Z \equiv \gamma_{LR}\gamma_{RR'}\gamma_{R'L} = ze^{-\imath\Omega/2}$, with z being the amplitude and $\Omega/2$ being the phase of the complex number Z which is the quantity of central focus. It essentially represents a series of cyclic projections $L \to R \to R' \to L$ forming a spherical triangle connected by three geodesics on the Bloch sphere [Fig. 3(b)]. The quantity Ω represents the solid angle subtended by this triangle at the center of the Bloch sphere and can be identified with Pancharatnam's geometric phase [17]. It should be noted that this phase can be tuned by altering the magnetization direction of the SPE leading to coherent oscillations in the current.

Now, we will discuss our protocol for observing these oscillations arising due to the Pancharatnam phase of geometric type which includes two measurable quantities: (a) the total average current injected into the edge states from the SPE, denoted as $I_{\rm tot}$, and (b) the current asymmetry ($I_{\rm diff}$) defined by the difference between the fractions of $I_{\rm tot}$ which flows to the left and right of the injection point (see Fig. 2). We can further assume a situation in which the SPE spinor $|n_{R'}\rangle$ lies on the x-y plane such that it is making an equal angle with that of the spin of right and left moving edge states, i.e., $|\gamma_{RR'}| = |\gamma_{LR'}| \equiv \alpha$. Such a situation remarkably simplifies

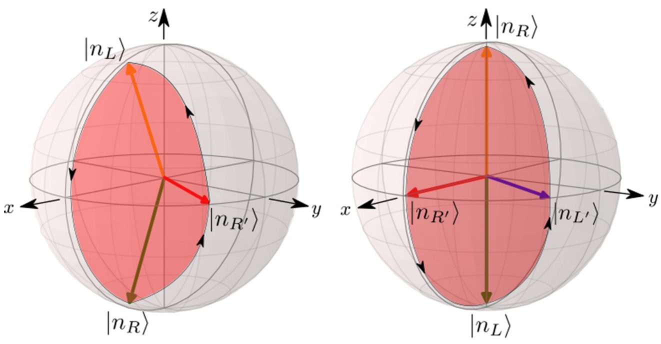

FIG. 3. (a) A triangular Pancharatnam loop formed by the geodesics connecting three spin states $|n_R\rangle$, $|n_L\rangle$, and $|n_{R'}\rangle$ on the Bloch sphere with orientation $L \rightarrow R \rightarrow R' \rightarrow L$. (b) A quadrilateral Pancharatnam loop formed by the geodesics connecting four spin states $|n_R\rangle$, $|n_L\rangle$, $|n_{R'}\rangle$, and $|n_{L'}\rangle$ on the Bloch sphere with orientation $R \rightarrow R' \rightarrow L \rightarrow L' \rightarrow R$. The solid angle subtended by the triangle or the quadrilateral loop at the center of the sphere is represented by Ω.

the expressions of I_{tot} and I_{diff} and brings out a dependence of current on the Pancharatnam phase. The expression for current in this situation is given by

$$\begin{aligned} I_{\text{tot}} &= \langle I_L^{\text{out}}\rangle + \langle I_R^{\text{out}}\rangle \\ &= \frac{e^2 V}{h} A\{2\alpha^2(4\hbar^2 v_F^2 + t^2|\gamma_{LR}|^2)\}t'^2, \end{aligned} \tag{7}$$

and

$$\begin{aligned} I_{\text{diff}} &= \langle I_L^{\text{out}}\rangle - \langle I_R^{\text{out}}\rangle \\ &= \frac{e^2 V}{h} A\left\{2t\hbar v_F|\gamma_{LR}|\alpha^2 \sin\frac{\Omega}{2}\right\}t'^2. \end{aligned} \tag{8}$$

Note that the expression of I_{tot} in Eq. (7) reduces to $I_{\text{tot}} = \frac{e^2 V}{h}t'^2$ for the case when the in-plane magnetic field acting on the edge is switched off and time-reversal symmetry is restored in the edge state leading to $|n_R\rangle = [1\ 0]^T$ and $|n_L\rangle = [0\ 1]^T$. Hence, the total current becomes independent of the magnetization angle of the SPE [28]. The ratio of the two directly measurable quantities I_{tot} in Eq. (7) to I_{diff} in Eq. (8) is given by

$$\mathcal{R} \equiv \left(\frac{\hbar v_F t|\gamma_{LR}|}{4\hbar^2 v_F^2 + t^2|\gamma_{LR}|^2}\right)\sin\frac{\Omega}{2}. \tag{9}$$

The current asymmetry parameter $\mathcal{R}$ is a particularly interesting quantity as it has no dependence on α or A and it only depends on γ_{LR} and Ω. This implies that we can induce oscillations in this quantity only by changing Ω by rotating the magnetization direction of the SPE while keeping γ_{LR} fixed. Hence this oscillation can be attributed purely to the variation of Pancharatnam's phase. At this point, it is apparent why, in order to detect Pancharatnam-type oscillations in interferometry, it is crucial to break the time-reversal symmetry on the edges of the QSHS, which renders $|\gamma_{LR}| \neq 0$. Also, these oscillations can be visualized as stretching the area of triangular Pancharatnam loops by tuning the magnetization direction of the tip alone [see Fig. 3(a)].

Similarly, the cross-correlated noise between the left and the right contact, which has the following expression [29]

$$\begin{aligned} S_{RL} = \frac{e^3}{h}\{&(s_{RR}^\dagger s_{RL} s_{LL}^\dagger s_{LR} + \text{H.c.})|V_R - V_L| \\ &+ (s_{RR}^\dagger s_{RR'} s_{LR'}^\dagger s_{LR} + \text{H.c.})|V_R - V_{R'}| \\ &+ (s_{RL}^\dagger s_{RR'} s_{LR'}^\dagger s_{LL} + \text{H.c.})|V_L - V_{R'}|\}, \end{aligned} \tag{10}$$

under the same condition as mentioned above reduces to

$$S_{RL} = 4\frac{e^3 V}{\pi\hbar}t'^4\alpha^4\left(A - A^2 t^2\hbar^2 v_F^2|\gamma_{LR}|^2 \sin^2\frac{\Omega}{2}\right) \tag{11}$$

to the leading order in t' [the expression of the quantity A is given right below Eq. (6)], and it evidently features oscillations via Pancharatnam's geometric phase as the currents in Eq. (6). This setup thus exemplifies an elegant noninterferometric platform where a Pancharatnam-type geometric phase is arising from one-particle interference (amplitude interferometry), that can be experimentally detected by simple mesoscopic measurements of current or noise. Hence, this completes addressing questions (a) and (b) raised in the Introduction by posting a physical situation which not only supports the local and controlled production of Pancharatnam's phase but also its manifestation in physical observables such as average current and dc current noise.

Finally, we note that t and $|\gamma_{LR}|$ always appear together as a product in the expressions of both current and noise. This is expected as a finite value of either of these implies breaking of the time-reversal invariance on the edges. Additionally, this product will continue to be a single parameter in our setup as long as the interedge bias $V_L - V_R = 0$ since it preserves the symmetry between the left and the right moving edges.

III. PANCHARATNAM PHASE IN INTENSITY INTERFEROMETRY

With this backdrop, we now address question (c) mentioned above. We study a setup comprising HES which is simultaneously coupled to two SPEs at the same spatial point on the edges [see Fig. 2(b)] such that it provides a *two-source two-detector* setup essential for observing intensity interferometry [13]. In this case, the current and noise would feature two-particle quadrilateral Pancharatnam loops unlike the triangular loops in the previous case as discussed below. We start with two SPEs with distinct polarization labeled R' and L' tunnel coupled with the QSHS, and their respective spin states are represented by $|n_{R'}\rangle$ and $|n_{L'}\rangle$. The tunneling Hamiltonian has the same form as Eq. (3) except that $\eta, \eta' \in \{R, L, R', L'\}$. We further assume the tunneling strength for both the SPEs to be the same (t'). The average currents and the noise are calculated with a voltage bias V applied to both the SPEs while the edge states are kept grounded. The current expressions $\langle I_\eta^{\text{out}}\rangle = \frac{e^2 V}{h}\sum_{\eta'}|s_{\eta\eta'}|^2$, where η can be R or L and $\eta' \in \{R', L'\}$, when explicitly written by substituting the corresponding S-matrix elements, take the forms

$$\begin{aligned}\langle I^{\rm out}_{(L/R)}\rangle &= \frac{e^2V}{h}\left\{\frac{t'^2}{\hbar^2 v_F^2}(|\gamma_{(L/R)R'}|^2+|\gamma_{(L/R)L'}|^2)\right.\\ &\quad+\frac{t'^4}{2\hbar^4 v_F^4}(|\gamma_{LR'}|^2|\gamma_{RR'}|^2+|\gamma_{LL'}|^2|\gamma_{RL'}|^2+(|\gamma_{(L/R)L'}|^2\\ &\quad\left.+|\gamma_{(L/R)R'}|^2)^2+\gamma_{RR'}\gamma_{R'L}\gamma_{LL'}\gamma_{L'R}+\text{H.c.})\right\}+O(t'^6),\end{aligned} \tag{12}$$

where we have considered time-reversal symmetric edge states, i.e., $\langle n_L|n_R\rangle = 0$. It should be noted that the presence of local backscattering ($t \neq 0$) is of no consequence for current $\langle I^{\rm out}_{(L/R)}\rangle$ as long as $\langle n_L|n_R\rangle = 0$ on the edges and $V_L - V_R = 0$ is maintained. Also from Eq. (12), we observe that Pancharatnam loops appear only in t'^4 order unlike the case of single SPE taking the form of geodesic quadrilaterals on the Bloch sphere with the four states in the order $R \to R' \to L \to L' \to R$ [see Fig. 3(b)]. Similarly, the cross-correlated noise between R and L obtained to t'^4 order (which is the leading order) reads as

$$\begin{aligned}S_{RL} &= -\frac{e^3V}{h}\frac{t'^4}{\hbar^4 v_F^4}\{|\gamma_{R'R}|^2|\gamma_{LR'}|^2+|\gamma_{L'R}|^2|\gamma_{LL'}|^2\\ &\quad+\gamma_{RR'}\gamma_{R'L}\gamma_{LL'}\gamma_{L'R}+\text{H.c.}\}.\end{aligned} \tag{13}$$

In this equation, the last term (and its H.c.), which represents a quadrilateral Pancharatnam loop, has a clear interpretation in terms of two-electron interference [29] where the two-particle amplitude for "SPE R' shooting an electron at the edge R and SPE L' shooting another electron at the edge L simultaneously" is interfering with the two-particle amplitude for "SPE R' shooting an electron at the edge L and SPE L' shooting another electron at the edge R simultaneously." This is precisely the reason why the leading-order contribution to cross-correlated noise comes at fourth order in t'.

Now, to observe manifestations of the Pancharatnam phase in currents and noise we start by considering an explicit choice for the spinors involved, $|n_R\rangle = [1\ 0]^T$ and $|n_L\rangle = [0\ 1]^T$, which can be represented by the north and south pole of the Bloch sphere [see Fig. 3(b)]. Next, we consider one of the SPEs' magnetization to be directed along the x axis so that $|n_{R'}\rangle = [1\ \ 1]^T/\sqrt{2}$ and the other SPE's magnetization is kept tunable in the x-y plane, which could give rise to oscillations in current and noise via the variation of Pancharatnam's geometric phase. We represent its spin state as $|n_{L'}\rangle = [1\ e^{\iota\phi}]^T/\sqrt{2}$. Then the expressions for the currents and noise reduce to

$$\langle I^{\rm out}_L\rangle = \langle I^{\rm out}_R\rangle = \frac{e^2V}{h}\left\{\frac{t'^2}{\hbar^2 v_F^2}+\frac{t'^4}{\hbar^4 v_F^4}\left(1+\cos^2\frac{\Omega'}{4}\right)\right\}, \tag{14}$$

and

$$S_{RL} = -\frac{e^3V}{h}\frac{t'^4}{\hbar^4 v_F^4}\cos^2\frac{\Omega'}{4}, \tag{15}$$

where $\Omega' = 2\phi$ is the solid angle subtended by the geodesic quadrilateral formed by the spin states $|n_R\rangle$, $|n_L\rangle$, $|n_{R'}\rangle$, and $|n_{L'}\rangle$ at the center of the Bloch sphere. Hence, by tuning ϕ, one can induce oscillations in the noise whose origin lies purely in the two-particle-type Pancharatnam's geometric phase as shown in Fig. 4. These oscillations have mild effects in current as the leading-order contribution appears in order t'^2 while the Ω'-dependent terms appear in the subleading order. On the other hand, in the case of cross-correlated noise they have dominant effects as they appear in the leading order itself, yielding oscillations in noise as a function of ϕ, as shown in Fig. 4.

Effects of orbital dephasing

As the mechanism to produce the interference pattern is local, it is expected to be robust and immune to the spatial dephasing in the system which we have explicitly verified in the two-SPE setup corresponding to the intensity interferometry. We include multiple tunneling points into the two-SPE setup and account for the dynamical phases picked up randomly by the electrons while traversing between consecutive tunneling points. Absorbing the phase factors appropriately requires converting the scattering matrices to transfer matrices (see the Appendix C) and multiply them in a path ordered fashion. The product is converted back to construct the scattering matrix corresponding to these multiple tunneling events. Averaging over the random phases then provides the model for an extended junction with a built-in orbital dephasing [30].

The results are presented in Fig. 5 in which we plot the noise in Eq. (15) as a function of the tuning parameter ϕ for the extended junction involving two SPEs and a certain number of tunneling points ($1 \leqslant n \leqslant 5$). The necessary calculations to include the dephasing effects are detailed in the Appendix C. The plot evinces the robustness of the oscillations against orbital dephasing. This fact can be of

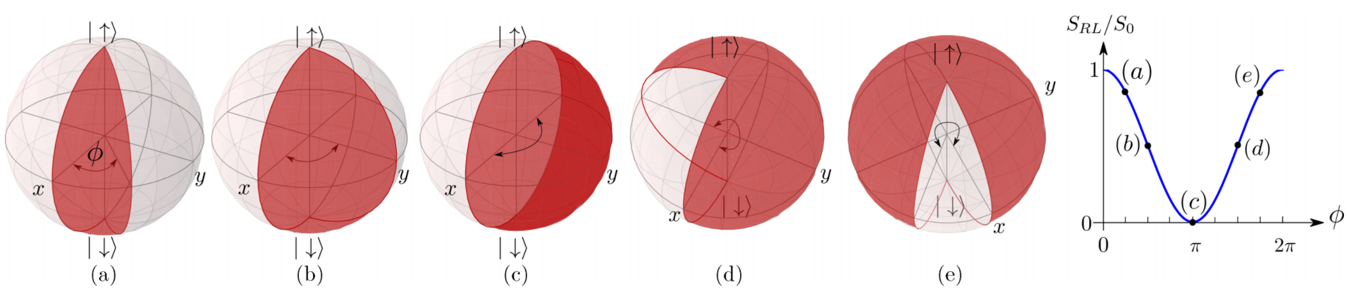

FIG. 4. (a)–(e) show the evolution of the quadrilateral Pancharatnam loop of Fig. 3(b) as ϕ varies for zero to 2π. The plot shows the variation of S_{RL} as a function of ϕ with $S_0 = (-e^3V/h)(t'^4/\hbar^4 v_F^4)$ being the prefactor in Eq. (15).

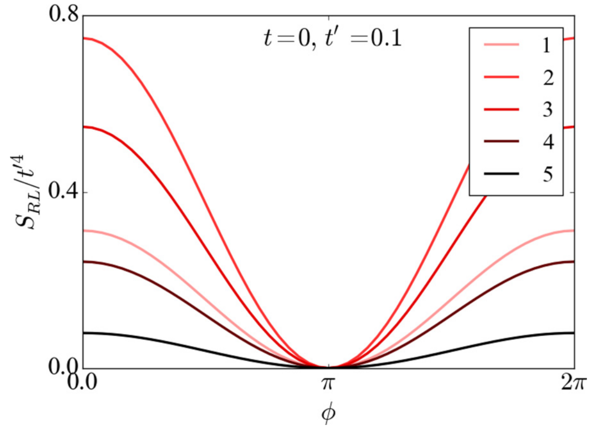

FIG. 5. The noise [scaled by a factor of t'^{-4} to compare with Eq. (15)] in the intensity interferometry setup measured as a function of the Pancharatnam phase ϕ as mentioned in Eq. (15) (with $\phi = \Omega'/2$) by including multiple tunneling points (the number shown in the legend), which reveals that these oscillations indeed survive orbital dephasing.

great importance as it can serve as a boon while exploring entanglement generation in such a setup by postselection [31] in the context of two-particle interferometers.

IV. DISCUSSION AND CONCLUSION

In the present paper, we explore the possibility of generating cyclic projective measurements on the spin-polarized states of the electron in a solid-state setting. We show that the quantum mechanical amplitude for tunneling an electron from a spin-polarized lead into a helical edge state depends naturally on the amplitudes [Z define below Eq. (6)] for cyclic projective measurements on the spin-polarized states of the electron. Hence the Pancharatnam-type geometric phase, which is the phase of the complex number Z, directly influences the tunneling current flowing from the spin-polarized lead into a helical edge state. In general, it will be rather difficult to perform a series of projective measurements via application of successive magnetic fields leading to the desired cyclic projective measurement on the electron spin and then perform interferometric measurements to read off the geometric phase. On the contrary, our setup leads to the generation of such a geometric phase via spatially local tunneling and also provides a possibility of detection via a tunneling current measurement. This is one of the important findings of this paper. As a next step, we consider a situation consisting of two such spin-polarized leads which are tunnel coupled to the helical edge state locally. Our motivation for considering such a scenario is to explore the possibilities of generating and measuring the HBT-type intensity-intensity correlations where the Pancharatnam-type geometric phase plays an essential role. With the HBT effect intrinsically being a two-electron effect, a connection to a Pancharatnam-type two-electron geometric phase is expected. This is precisely what has been elucidated in this paper. The cross-correlated current noise between the two SPEs in our setup features coherent oscillations only due to its direct dependence on a Pancharatnam-type two-electron geometric phase. The oscillations, which are found remarkably robust against orbital dephasing, are not expected to appear unless the HBT correlations dominate the signal.

Lastly, it is worth noting that the HBT effect has to do with the interference between independent two-electron processes which are indistinguishable. Our setup uses a spin-polarized lead with distinct polarization direction as a source of electrons and hence might give an apparent impression that this fact will lead to distinguishability of different interfering amplitudes leading to suppression of the HBT effect. This is not the case for us because the tunneling process in our proposed setup does break spin rotational symmetry about all axes. When the electron tunnels into the helical edge from any of the two spin-polarized leads, the only choice it is left with is to become spin polarized along the $|n_R\rangle$ or $|n_L\rangle$ direction depending on if it tunneled into the left moving edge state or the right moving one. Hence the electron's initial polarization becomes irrelevant as far as distinguishability of the electron based on its initial spin polarization is concerned.

ACKNOWLEDGMENTS

S.D. would like to thank Michael V. Berry for enlightening conversations related to the Pancharatnam phase, N. Mukunda for clarifying some subtleties associated with representing multiphoton polarization states on a Poincaré sphere [9], and a discussion on the possible implications for an electronic counterpart, and Mikhail Kiselev for useful discussions. The work of P.M. is supported by funding from the University Grants Commission under the second phase of University with Potential of Excellence (UPE II) and DST-PURSE grant at JNU from the Department of Science and Technology. S.D. would like to acknowledge Ministry of Human Resource Development for generous funding and IISER Kolkata for the research facilities. K.R. acknowledges support in part by the National Science Foundation under Grant No. NSF PHY17-48958. The authors would like to acknowledge the kind hospitality from the Theory Group at the European Organization for Nuclear Research, CERN, Geneva (P.M.) and Abdus Salam International Centre for Theoretical Physics, Trieste under the associate scheme (S.D.) during crucial stages of this work.

APPENDIX A: SCATTERING MATRIX FOR AMPLITUDE INTERFEROMETRY

The scattering amplitude for a wave function ψ_η with $\eta \in \{R, L, R'\}$ across the point contact can be obtained by studying its equation of motion (EOM) [27]

$$\imath\hbar\dot{\psi}_\eta = [\psi_\eta, \mathcal{H}], \tag{A1}$$

where $\mathcal{H}$ is given in Eq. (4). Integrating the EOM over a region from $-\epsilon$ and ϵ with the limit $\epsilon \to 0$, one obtains the following set of equations,

$$\begin{aligned}\psi_R(0^+) - \psi_R(0^-) &= -\imath\Gamma_{RR'}\{\psi_{R'}(0^+) + \psi_{R'}(0^-)\}/2\\ &\quad - \imath\Gamma_{RL}\{\psi_L(0^+) + \psi_L(0^-)\}/2,\\ \psi_L(0^+) - \psi_L(0^-) &= \imath\Gamma_{LR'}\{\psi_{R'}(0^+) + \psi_{R'}(0^-)\}/2\\ &\quad + \imath\Gamma^*_{RL}\{\psi_R(0^+) + \psi_R(0^-)\}/2,\\ \psi_{R'}(0^+) - \psi_{R'}(0^-) &= -\imath\Gamma^*_{RR'}\{\psi_R(0^+) + \psi_R(0^-)\}/2\\ &\quad - \imath\Gamma^*_{LR'}\{\psi_L(0^+) + \psi_L(0^-)\}/2,\end{aligned} \tag{A2}$$

where we have used $\psi_\eta = \{\psi_\eta(0^+) + \psi_\eta(0^-)\}/2$ and $\Gamma_{\eta\eta'}$ is a dimensionless parameter defined as $\Gamma_{\eta\eta'} \equiv t_{\eta\eta'}/\hbar v_F$ [see Eq. (3) for the definition of $t_{\eta\eta'}$]. We can now define the S-matrix elements for each of the modes which can be explicitly calculated from a set of three equations for each of them. For example, an electron on the right moving edge (R) can either scatter to the left edge (L) or to the SPE (R'), or reflect along the same edge. Accordingly, we define the respective amplitudes $s_{LR} = \psi_L(0^-)/\psi_R(0^-)$, $s_{R'R} = \psi_{R'}(0^+)/\psi_R(0^-)$, and $s_{RR} = \psi_R(0^+)/\psi_R(0^-)$ which satisfy the following equations [derived from Eq. (A2)],

$$\begin{aligned} s_{RR} - 1 &= -\frac{\iota}{2}\Gamma_{RR'}s_{R'R} - \frac{\iota}{2}\Gamma_{RL}s_{LR},\\ s_{LR} &= -\frac{\iota}{2}\Gamma_{LR'}s_{R'R} - \frac{\iota}{2}\Gamma^*_{RL}(s_{RR}+1),\\ s_{R'R} &= -\frac{\iota}{2}\Gamma^*_{LR'}s_{LR} - \frac{\iota}{2}\Gamma^*_{RR'}(s_{RR}+1). \end{aligned} \tag{A3}$$

Similarly, scattering from a left mover (L) would have

$$\begin{aligned} s_{RL} &= -\frac{\iota}{2}\Gamma_{RR'}s_{R'L} - \frac{\iota}{2}\Gamma_{RL}(s_{LL}+1),\\ s_{LL} - 1 &= -\frac{\iota}{2}\Gamma_{LR'}s_{R'L} - \frac{\iota}{2}\Gamma^*_{RL}s_{RL},\\ s_{R'L} &= -\frac{\iota}{2}\Gamma^*_{LR'}(s_{LL}+1) - \frac{\iota}{2}\Gamma^*_{RR'}s_{RL}, \end{aligned} \tag{A4}$$

where $s_{RL} = \psi_R(0^+)/\psi_L(0^+)$, $s_{R'L} = \psi_{R'}(0^+)/\psi_L(0^+)$, and $s_{LL} = \psi_L(0^-)/\psi_L(0^+)$, and for the SPE ($R'$) we get

$$\begin{aligned} s_{RR'} &= -\frac{\iota}{2}\Gamma_{RR'}(s_{R'R'}+1) - \frac{\iota}{2}\Gamma_{RL}s_{LR'},\\ s_{LR'} &= -\frac{\iota}{2}\Gamma_{LR'}(s_{R'R'}+1) - \frac{\iota}{2}\Gamma^*_{RL}s_{RR'},\\ s_{R'R'} - 1 &= -\frac{\iota}{2}\Gamma^*_{LR'}s_{LR'} - \frac{\iota}{2}\Gamma^*_{RR'}s_{RR'}, \end{aligned} \tag{A5}$$

where $s_{LR'} = \psi_L(0^-)/\psi_{R'}(0^-)$, $s_{R'R'} = \psi_{R'}(0^+)/\psi_{R'}(0^-)$, and $s_{RR'} = \psi_R(0^+)/\psi_{R'}(0^-)$. Solving Eqs. (A3)–(A5) together, we can obtain an explicit expression for each of the $s_{\eta\eta'}$ (η, η' can be R, L, or R') defined above which constitute the full S matrix in Eq. (5) as

$$\underbrace{\begin{pmatrix}\psi_R(0^+)\\ \psi_L(0^-)\\ \psi_{R'}(0^+)\end{pmatrix}}_{\psi^{\text{out}}} = \underbrace{\begin{pmatrix} s_{RR} & s_{RL} & s_{RR'}\\ s_{LR} & s_{LL} & s_{LR'}\\ s_{R'R} & s_{R'L} & s_{R'R'}\end{pmatrix}}_{S\text{-matrix}} \underbrace{\begin{pmatrix}\psi_R(0^-)\\ \psi_L(0^+)\\ \psi_{R'}(0^-)\end{pmatrix}}_{\psi^{\text{in}}}. \tag{A6}$$

The explicit expressions for the S-matrix elements are given by

$$\begin{aligned} s_{RR} = [8 &+ \iota(\Gamma_{RL}\Gamma^*_{RR'}\Gamma_{LR'} + \Gamma^*_{RL}\Gamma_{RR'}\Gamma^*_{LR'})\\ &- 2\{|\Gamma_{RL}|^2 + |\Gamma_{RR'}|^2 - |\Gamma_{LR'}|^2\}]/D, \end{aligned} \tag{A7}$$

$$s_{RL} = [-8\iota\Gamma_{RL} - 4\Gamma_{RR'}\Gamma^*_{LR'}]/D, \tag{A8}$$

$$s_{RR'} = [-8\iota\Gamma_{RR'} - 4\Gamma_{RL}\Gamma_{LR'}]/D, \tag{A9}$$

$$s_{LR} = [-8\iota\Gamma^*_{RL} - 4\Gamma^*_{RR'}\Gamma_{LR'}]/D, \tag{A10}$$

$$\begin{aligned} s_{LL} = [8 &+ \iota(\Gamma_{RL}\Gamma^*_{RR'}\Gamma_{LR'} + \Gamma^*_{RL}\Gamma_{RR'}\Gamma^*_{LR'})\\ &- 2\{|\Gamma_{RL}|^2 - |\Gamma_{RR'}|^2 + |\Gamma_{LR'}|^2\}]/D, \end{aligned} \tag{A11}$$

$$s_{LR'} = [-8\iota\Gamma_{LR'} - 4\Gamma^*_{RL}\Gamma_{RR'}]/D, \tag{A12}$$

$$s_{R'R} = [-8\iota\Gamma^*_{RR'} - 4\Gamma^*_{RL}\Gamma^*_{LR'}]/D, \tag{A13}$$

$$s_{R'L} = [-8\iota\Gamma^*_{LR'} - 4\Gamma_{RL}\Gamma^*_{RR'}]/D, \tag{A14}$$

$$\begin{aligned} s_{R'R'} = [8 &+ \iota(\Gamma_{RL}\Gamma^*_{RR'}\Gamma_{LR'} + \Gamma^*_{RL}\Gamma_{RR'}\Gamma^*_{LR'})\\ &- 2\{-|\Gamma_{RL}|^2 + |\Gamma_{RR'}|^2 + |\Gamma_{LR'}|^2\}]/D, \end{aligned} \tag{A15}$$

where the common denominator D is

$$\begin{aligned} D = 8 &- \iota(\Gamma_{RL}\Gamma^*_{RR'}\Gamma_{LR'} + \Gamma^*_{RL}\Gamma_{RR'}\Gamma^*_{LR'})\\ &+ 2\{|\Gamma_{RL}|^2 + |\Gamma_{RR'}|^2 + |\Gamma_{LR'}|^2\}. \end{aligned} \tag{A16}$$

APPENDIX B: SCATTERING MATRIX FOR INTENSITY INTERFEROMETRY

The S matrix for this case is given by

$$\underbrace{\begin{pmatrix}\psi_R(0^+)\\ \psi_{R'}(0^-)\\ \psi_L(0^+)\\ \psi_{L'}(0^-)\end{pmatrix}}_{\psi^{\text{out}}} = \underbrace{\begin{pmatrix} s_{RR} & s_{RR'} & s_{RL} & s_{RL'}\\ s_{R'R} & s_{R'R'} & s_{R'L} & s_{R'L'}\\ s_{LR} & s_{LR'} & s_{LL} & s_{LL'}\\ s_{L'R} & s_{L'R'} & s_{L'L} & s_{L'L'}\end{pmatrix}}_{S-\text{matrix}} \underbrace{\begin{pmatrix}\psi_R(0^-)\\ \psi_{R'}(0^+)\\ \psi_L(0^-)\\ \psi_{L'}(0^+)\end{pmatrix}}_{\psi^{\text{in}}}, \tag{B1}$$

where expressions for the individual elements are obtained by solving the following set of equations,

$$\begin{aligned} s_{RR} - 1 &= -\frac{\iota}{2}[\Gamma_{RR'}s_{R'R} + \Gamma_{RL'}s_{L'R} + \Gamma_{RL}s_{LR}],\\ s_{LR} &= -\frac{\iota}{2}[\Gamma_{LR'}s_{R'R} + \Gamma_{LL'}s_{L'R} + \Gamma_{LR}(s_{RR}+1)], \end{aligned} \tag{B2}$$

$$\begin{aligned} s_{R'R} &= -\frac{\iota}{2}[\Gamma_{R'L}s_{LR} + \Gamma_{R'R}(s_{RR}+1)],\\ s_{L'R} &= -\frac{\iota}{2}[\Gamma_{L'L}s_{LR} + \Gamma_{L'R}(s_{RR}+1)],\\ s_{LL} - 1 &= -\frac{\iota}{2}[\Gamma_{LR'}s_{R'L} + \Gamma_{LL'}s_{L'L} + \Gamma_{LR}s_{RL}],\\ s_{RL} &= -\frac{\iota}{2}[\Gamma_{RR'}s_{R'L} + \Gamma_{RL'}s_{L'L} + \Gamma_{RL}(s_{LL}+1)], \end{aligned} \tag{B3}$$

$$\begin{aligned} s_{R'L} &= -\frac{\iota}{2}[\Gamma_{R'R}s_{RL} + \Gamma_{R'L}(s_{LL}+1)],\\ s_{L'L} &= -\frac{\iota}{2}[\Gamma_{L'R}s_{RL} + \Gamma_{L'L}(s_{LL}+1)],\\ s_{RR'} &= -\frac{\iota}{2}[\Gamma_{RL'}s_{L'R'} + \Gamma_{RL}s_{LR'} + \Gamma_{RR'}(s_{R'R'}+1)],\\ s_{LR'} &= -\frac{\iota}{2}[\Gamma_{LL'}s_{L'R'} + \Gamma_{LR}s_{RR'} + \Gamma_{LR'}(s_{R'R'}+1)], \end{aligned} \tag{B4}$$

$$\begin{aligned} s_{R'R'} - 1 &= -\frac{\iota}{2}[\Gamma_{R'R}s_{RR'} + \Gamma_{R'L}s_{LR'}],\\ s_{L'R'} &= -\frac{\iota}{2}[\Gamma_{L'R}s_{RR'} + \Gamma_{L'L}s_{LR'}], \end{aligned}$$

$$\begin{aligned}
s_{RL'} &= -\frac{\iota}{2}[\Gamma_{RR'}s_{R'L'} + \Gamma_{RL}s_{LL'} + \Gamma_{RL'}(s_{L'L'}+1)],\\
s_{LL'} &= -\frac{\iota}{2}[\Gamma_{LR'}s_{R'L'} + \Gamma_{LR}s_{RL'} + \Gamma_{LL'}(s_{L'L'}+1)],\\
s_{R'L'} &= -\frac{\iota}{2}[\Gamma_{R'R}s_{RL'} + \Gamma_{R'L}s_{LL'}],\\
s_{L'L'} - 1 &= -\frac{\iota}{2}[\Gamma_{L'R}s_{RL'} + \Gamma_{L'L}s_{LL'}]. \qquad \text{(B5)}
\end{aligned}$$

The explicit forms are too complicated to write here.

APPENDIX C: MODELING THE EXTENDED JUNCTION

An extended junction in the interferometer geometry features multiple tunneling events, each of which is described by the S matrix in Eq. (B1) for the two-SPE setup. However, to construct the composite S matrix including all such processes, one needs to resort to the transfer matrix (M) approach which involves the following steps:

(1) Convert the S matrix to a M matrix defined through

$$\psi_\eta^{\text{right}} = \sum_{\eta'} m_{\eta\eta'}\, \psi_{\eta'}^{\text{left}}, \qquad \text{(C1)}$$

where $\psi^{\text{left}} = [\psi_R(0^-), \psi_{R'}(0^-), \psi_L(0^-), \psi_{L'}(0^-)]^T$ and $\psi^{\text{right}} = [\psi_R(0^+), \psi_{R'}(0^+), \psi_L(0^+), \psi_{L'}(0^+)]^T$. In this basis, one can write

$$S = \begin{pmatrix} U & V' \\ V & U' \end{pmatrix}, \qquad \text{(C2)}$$

and define the transfer matrix as

$$M \equiv \begin{pmatrix} P & Q' \\ Q & P' \end{pmatrix}, \qquad \text{(C3)}$$

where U, U', V, V', P, P', and Q, Q' are all 2×2 blocks. The transformation relation from S to M is straightforward to calculate, which reads

$$\begin{aligned}
P &= U - V'\cdot U'^{-1}\cdot V,\\
Q &= -U'^{-1}\cdot V,\\
P' &= U'^{-1},\\
Q' &= V'\cdot U'^{-1},
\end{aligned} \qquad \text{(C4)}$$

which provide the explicit expression for $m_{\eta\eta'}$ in Eq. (C1).

(2) Account for the random dynamical phases (θ_D) picked up by the wave functions between two consecutive tunneling events. This is encoded in the scattering matrix

$$S^P = \begin{pmatrix} e^{\iota\theta_D}\mathbb{I}_{2\times 2} & 0 \\ 0 & e^{-\iota\theta_D}\mathbb{I}_{2\times 2} \end{pmatrix}. \qquad \text{(C5)}$$

Construct the composite transfer matrix for the extended junction as

$$M \equiv M_1 \cdot M_1^P \cdot M_2 \cdot M_2^P \cdots M_n, \qquad \text{(C6)}$$

where n consecutive tunneling events are considered to take place during the scattering process through the extended junction and M^P is the transfer matrix obtained from S^P in Eq. (C5).

Finally, the composite scattering matrix (S) for the extended junction can be constructed back following

$$\begin{aligned}
U &= P - Q'\cdot P'^{-1}\cdot Q,\\
V &= -P'^{-1}\cdot Q,\\
U' &= P'^{-1},\\
V' &= Q'\cdot P'^{-1}.
\end{aligned} \qquad \text{(C7)}$$

To observe the effects of orbital dephasing on the measurable quantities calculated from S for this extended junction, one needs to average over all the random phases given by $\{\theta_D\}$ [30]. The results obtained following this procedure in regard to calculating the noise in the intensity interferometer setup are presented in Fig. 5.

[1] M. V. Berry, Proc. R. Soc. London, Ser. A **392**, 45 (1984).
[2] S. Ramaseshan and R. Nityananda, Curr. Sci. **55**, 1225 (1986).
[3] S. Pancharatnam, Proc. Indian Acad. Sci. A **44**, 247 (1956).
[4] Y. Aharonov and D. Bohm, Phys. Rev. **115**, 485 (1959).
[5] M. Berry, J. Mod. Opt. **34**, 1401 (1987).
[6] P. Mehta, Phys. Rev. D **79**, 096013 (2009).
[7] R. Hanbury Brown and R. Q. Twiss, Nature (London) **178**, 1046 (1956).
[8] P. Mehta, J. Samuel, and S. Sinha, Phys. Rev. A **82**, 034102 (2010).
[9] Arvind, S. Chaturvedi, and N. Mukunda, Phys. Lett. A **381**, 1272 (2017).
[10] A. Martin, O. Alibart, J.-C. Flesch, J. Samuel, S. Sinha, S. Tanzilli, and A. Kastberg, Europhys. Lett. **97**, 10003 (2012).
[11] N. Satapathy, D. Pandey, P. Mehta, S. Sinha, J. Samuel, and H. Ramachandran, Europhys. Lett. **97**, 50011 (2012).
[12] I. Neder, N. Ofek, Y. Chung, M. Heiblum, D. Mahalu, and V. Umansky, Nature (London) **448**, 333 (2007).
[13] P. Samuelsson, E. V. Sukhorukov, and M. Büttiker, Phys. Rev. Lett. **92**, 026805 (2004).
[14] Y. Ji, Y. Chung, D. Sprinzak, M. Heiblum, D. Mahalu, and H. Shtrikman, Nature (London) **422**, 415 (2003).
[15] This can happen either due to a nonuniform magnetic field acting on the arms of the interferometer [19,32] or due to the presence of spin-orbit coupling [33] in the arms of the interferometer. As the purpose of this discussion is to illustrate the essential physics of a specific kind of AB effect, we refrain from going into the details of the specific model responsible for inducing the rotation of the spin.
[16] J. Maciejko, E.-A. Kim, and X.-L. Qi, Phys. Rev. B **82**, 195409 (2010).
[17] J. Samuel and R. Bhandari, Phys. Rev. Lett. **60**, 2339 (1988).
[18] D. Loss and P. M. Goldbart, Phys. Rev. B **45**, 13544 (1992).
[19] A. Stern, Phys. Rev. Lett. **68**, 1022 (1992).
[20] C. L. Kane and E. J. Mele, Phys. Rev. Lett. **95**, 226801 (2005).
[21] C. L. Kane and E. J. Mele, Phys. Rev. Lett. **95**, 146802 (2005).

[22] B. A. Bernevig and S.-C. Zhang, Phys. Rev. Lett. **96**, 106802 (2006).
[23] B. A. Bernevig, T. L. Hughes, and S.-C. Zhang, Science **314**, 1757 (2006).
[24] C. Brüne, A. Roth, H. Buhmann, E. M. Hankiewicz, L. W. Molenkamp, J. Maciejko, X.-L. Qi, and S.-C. Zhang, Nat. Phys. **8**, 485 (2012).
[25] D. Wadhawan, P. Mehta, and S. Das, Phys. Rev. B **93**, 085310 (2016).
[26] C.-Y. Hou, K. Shtengel, and G. Refael, Phys. Rev. B **88**, 075304 (2013).
[27] C. Mahaux and H. A. Weidenmüller, Phys. Rev. **170**, 847 (1968).
[28] S. Das and S. Rao, Phys. Rev. Lett. **106**, 236403 (2011).
[29] Y. M. Blanter and M. Büttiker, Phys. Rep. **336**, 1 (2000).
[30] S. Pilgram, P. Samuelsson, H. Förster, and M. Büttiker, Phys. Rev. Lett. **97**, 066801 (2006).
[31] K. Roychowdhury, D. Wadhawan, P. Mehta, B. Karmakar, and S. Das, Phys. Rev. B **93**, 220101 (2016).
[32] D. Loss, P. Goldbart, and A. V. Balatsky, Phys. Rev. Lett. **65**, 1655 (1990).
[33] S. Datta and B. Das, Appl. Phys. Lett. **56**, 665 (1990).